

Spatio-temporal visualization of light transport in complex photonic structures

Lorenzo Pattelli^{*1}, Romolo Savo^{†1}, Matteo Burrelli^{‡2}, and
Diederik S. Wiersma^{1,3}

¹*European Laboratory for Non-linear Spectroscopy (LENS), Università di Firenze, 50019 Sesto Fiorentino (FI), Italy*

²*Istituto Nazionale di Ottica (CNR-INO), Largo Fermi 6, 50125 Firenze (FI), Italy*

³*Università di Firenze, Dipartimento di Fisica e Astronomia, 50019 Sesto Fiorentino (FI), Italy*

Spatio-temporal imaging of light propagation is of significant importance in photonics, since it provides the most direct tool for studying the interaction between light and its host environment. Sub-ps time resolution is needed to appreciate fine and complex structural features as those occurring in disordered and heterogeneous structures, which are responsible for a rich transport physics that still needs to be fully explored. Thanks to a newly developed wide-field imaging system we present a spatio-temporal study on light transport in various disordered media, revealing properties that could not be properly assessed with standard techniques. By extending our investigation to an almost transparent membrane — a configuration which would be hardly possible to characterize to date — we unveil the peculiar physics exhibited by such thin scattering systems, with transport features that go beyond mainstream diffusion modeling despite the occurrence of multiple scattering.

Introduction

Light represents a useful and versatile probe to study our world. By tracking its evolution in the domain of time, space, frequency and reciprocal space we are indeed able to extract a wealth of information regarding its surrounding environment. Further insight is often gained when we become technically able to track this evolution in more than one such domains simultaneously, as demonstrated by a number of results recently coming from the most diverse research fields^{1–8}. Among different approaches, spatio-temporally resolved techniques undoubtedly offer

^{*}Corresponding author

[†]Current affiliation: *Laboratoire Kastler Brossel, UMR 8552, CNRS, Ecole Normale Supérieure, Université Pierre et Marie Curie, Collège de France, 24 rue Lhomond, 75005 Paris, France*

[‡]Current position: *Gestione SILO Srl, via di Castelpulci 14/d, 50010 Scandicci (FI), Italy*

the most straightforward picture, as underlined by the continuously growing interest in ultrafast photography^{9–11} and imaging^{12–15} applications. Further development of similar techniques is key to our ability to investigate increasingly more complex media such as disordered or heterogeneous media which are ubiquitous in most fields of study, from atmospheric physics to biology and cultural heritage preservation. In this context, achieving sub-ps time resolution allows not only to study minute or thin specimens, but opens the possibility to address the very first scattering events, which are predicted to reveal fine structural features hardly accessible otherwise¹⁶.

In the case of disordered media, repetitive techniques are especially sought after as they provide the most convenient way to non-invasively probe and average over their properties. Yet, the ultrafast time resolution needed for such applications still represents an experimental challenge. Established fast imaging techniques involve electronic-based devices as streak cameras or sequentially scanning over a given sample in a pump-probe configuration. Despite providing very accurate results, many of these techniques are limited by a low time resolution¹³ or a long acquisition time¹⁵. On the contrary, wide-field images at sub-ps time scales are easily obtained with optical gating techniques, but their limited accuracy has limited their use to qualitative pattern/shadowgram recognition rather than absolute intensity measurement across the whole field of view. In other words, gating has been exploited so far just as a convenient method to see through a turbid medium obliterating the complex light transport arising from its structure, rather than to tackle its study directly.

To fill this gap, in this work we studied light transport focusing in particular on three classes of disordered media which are extremely relevant for practical applications and yet still very difficult to characterize accurately, namely samples with limited thickness, large scale heterogeneities and semi-transparent membranes. In each of these cases, transport properties are retrieved exploiting for the first time an all-optical gating setup which we purposely developed aiming at offering both a wide field acquisition and a high quantitative accuracy on a sub-ps time scale. Our spatio-temporal investigation allowed to grasp the evolution of light transport in its entirety, thus unveiling effects that were either overlooked or misinterpreted to date, including a peculiar transport regime occurring in ultra-thin disordered media that becomes apparent only when the spatial and temporal domain can be studied simultaneously, and would hardly be detectable with other state-of-the-art techniques. By comparing the outcome of our analysis with that of the mainstream evaluation model based on the diffusive approximation, we describe how single-domain investigations performed to date are susceptible to particularly deceiving artifacts which can instead be clearly appreciated from a multi-domain set of data. At the same time, as widely suggested in the literature, we discuss how a much more robust interpretation — even within the diffusive framework — can be given in terms of transverse transport, which our technique grants direct access to.

Materials and Methods

Experimental setup The optical scheme employed to resolve in time and space light propagation in complex media is based on the cross-correlation gating technique^{17,18} as schematically shown in Fig. 1a. Two synchronous, collinear probe and gate pulses at different wavelengths

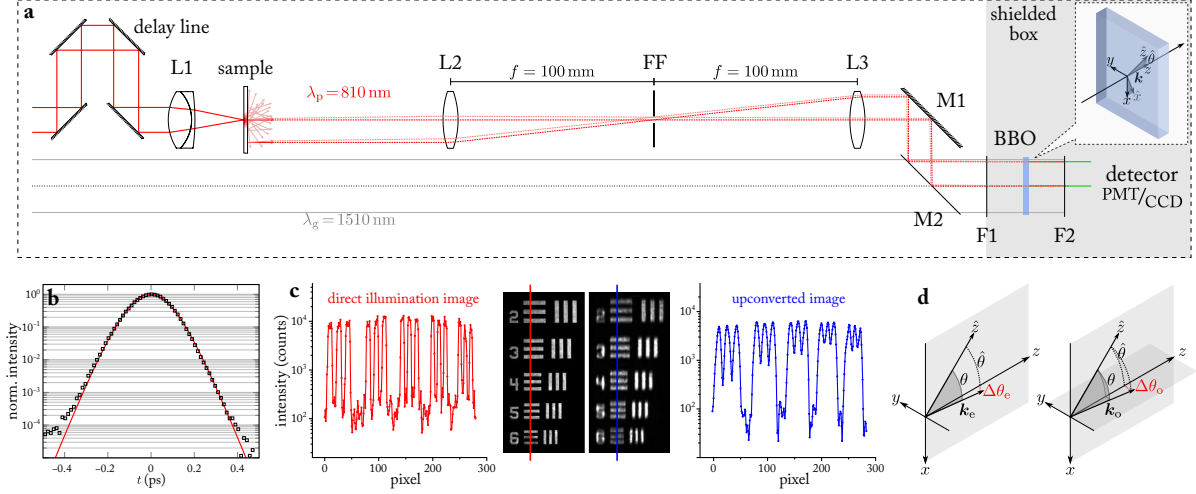


Figure 1: Experimental setup and spatio-temporal resolution. **a** Two linearly polarized fs-pulses are provided by a Ti:Sa laser (probe, red) and a synchronously pumped OPO (gate, gray). The probe beam interacts with a slab sample which is imaged on a BBO crystal by a $4f$ lens configuration. A Fourier filter (FF) allows to filter k vectors isotropically while a dichroic mirror (M2) guarantees signal and gate spatial superposition. A long-pass (F1) and a bandpass filter (F2) block visible and unconverted light respectively. **b** Typical cross-correlation time-resolved measurement acquired with a photomultiplier tube (PMT). A fit with the cross-convolution of two sech^2 pulses returns a FWHM of 174 fs. **c** The spatial information carried by the pulse is retrieved by a CCD camera with a resolution influenced by the sum-frequency process. **d** Geometric sketch showing qualitatively how the phase-matching condition results in different angular acceptances along the extraordinary and ordinary direction: a slightly misaligned k_e and a largely misaligned k_o might give the same $\Delta\theta$, thus explaining the sharper resolution along the y direction.

are made to impinge on a 2 mm thick β -Barium borate (BBO) crystal. When the two beams overlap both spatially and temporally, a sum-frequency signal is generated with an intensity proportional to the cross-correlation of the original pulses as a function of a delay-line position. This technique has been used to fully characterize ultrafast pulse propagation^{19–21}, generally disregarding the spatial distribution of the converted signal (cfr. Fig. 1b). Nevertheless, cross-correlation gating techniques offer several advantages, as being unaffected by optical chirp (in contrast with interferometric methods) and compatible with a collinear scheme. This helps mitigating possible distortion of the up-converted images through the BBO, which is a crucial aspect for accurate spatially resolved experiments²².

Upconversion imaging In order to study the dynamics of light emerging from a complex specimen we image its exit surface on the BBO crystal, which up-converts this image to a different wavelength once that the gate pulse impinges simultaneously with the probe pulse on the BBO crystal. Non-linear up-conversion is a polarization- and wavevector-sensitive process, and both these aspects must be taken carefully into account while designing an imaging apparatus. In the specific case of the current investigations which deals with multiply scattering systems, the polarization sensitivity is not relevant since any polarization channel has the same optical properties. However, it has to be noted that the setup inherently allows to investigate different polarization channels separately. As regards the phase matching condition, the BBO converts only those wavevectors laying within a relatively narrow paraxial window in reciprocal space, which defines the angular acceptance of the BBO. This acceptance angle is weighted differently along the x - and y -direction of the BBO surface (i.e., along the image plane, see Figs. 1c and d). A double telecentric optical apparatus ensures that the paraxial component emerging from the sample is preserved at the crystal interface. By doing so one obtains a quantitatively accurate reproduction of the original intensity distribution at each time step for each point of the object field: the accuracy condition is verified as long as the transmitted wavevector distribution — however complex — does not depend on the point and time of exit, as it is well the case with disordered samples as far as quasi-ballistic light is excluded. The insertion of an iris (FF) in the Fourier plane of the collecting lens acts as a tunable isotropic wavevector filter. For our experiment we choose a $4f$ lens configuration to have a $1\times$ magnification.

As can be qualitatively seen from Figure 1c, the reduced set of available wavevectors degrades the sharpness of the retrieved image differently along the two axes. In order to obtain the same resolving power along both x and y directions the Fourier filter can be closed accordingly. Several alternative up-converting configurations are reported in the literature regarding full-frame imaging applications^{6,23–30}, most of which employ the non-linear crystal in the Fourier plane of the imaging optics rather than in the image plane. Both configurations present different advantages and their adoption is to be preferred depending on the specific application. In the common Fourier-plane configuration the angular acceptance limits up-conversion uniformity over the whole field of view, while in our case the image is formed with a cut-off set of k vectors (thus the lower resolution) while guaranteeing a spatially uniform up-conversion efficiency. We therefore adopted the latter configuration since our diffuse signal typically does not exhibit any sharp feature, while a spatially uniform response represents a critical condition to attain

our quantitative accuracy goal over multiple orders of magnitude. The generated signal is eventually collected by a lens inside a shielded box where a flip mirror allows to switch between different detection schemes.

We initially performed standard time-resolved measurements by using a photon counter (PMT), i.e. collecting intensity without any spatial resolution. Figure 1b shows a typical cross-correlation measurement of our probe pulse passing through a test target, together with a fit obtained as the convolution of two squared hyperbolic secant functions (see SI). The measurement does not exhibit any relevant satellite over several orders of magnitude. By switching the photon counter with a CCD camera a transient image is detected (Fig. 1c) showing the spatial resolution of our setup ($\sim 11.3 \text{ lp mm}^{-1}$ at 0.5 contrast), comparable with previous publications^{6,25,27,30}.

Data evaluation models Applying an ultrafast imaging technique to the study of light transport in a complex environment provides an incredibly rich picture. Especially in the case of disordered media, the amount of information that a full spatio-temporal investigation outputs is hardly taken into account by commonly used data evaluation procedures. Exact modeling of energy transport in disordered samples is provided by the Radiative Transfer Equation (RTE), in which light propagation can be modeled as a random walk of energy packets undergoing scattering and absorption events. The characteristic length l_s over which a packet on average is scattered is called the scattering mean free path, while the anisotropic scattering factor g expresses the average degree of scattering directionality ranging between completely random ($g = 0$) and perfectly forward ($g = 1$). These parameters are directly linked to the internal structure of the sample and the properties of its basic scattering elements and as such are the physical quantities of interest to retrieve in any light transport measurement. However, a so-called similarity relation exists^{31,32} equating a random walk with certain l_s and g to a completely isotropic random walk with a rescaled mean free path $l_t = l_s/(1 - g)$. Thanks to this relation very often light transport is studied in the isotropic diffusion approximation (DA) regime, where a single diffusion coefficient $D = l_t v/3$ is used as the only transport parameter, with a consequent loss of insight on the microscopic scattering properties of the sample. Moreover, the convenient description offered by the diffusive approximation is known to be valid only when the transport mean free path is much smaller than the sample size. On the contrary, its applicability to optically thin media is often debated and a standard approach to measure transport parameters in this regime is still missing. Several efforts have been made to find extensions of the diffusive model for optically thin media^{33–35} and alternative techniques to measure transport parameters have been proposed, which however skip its use completely^{36–44} and are mainly based on single domain (e.g. temporal, spatial, angular, etc.) investigations.

In this work we analyze our experimental data both with the mainstream diffusion theory and with a Monte Carlo modeling of light transport, for comparison. While the former still retains a large appeal due to its simplicity, the latter represents a direct implementation of the radiative transfer theory, providing a more computationally expensive but asymptotically exact solution to the transport problem. This allows us to unveil some particularly deceptive ways in which the diffusive approximation can fail when dealing with certain kinds of media.

Results and Discussion

In the following paragraphs we present a few relevant experimental cases where, exploiting our newly developed UltraFast Imaging (UFI) setup, we are able to reveal structural and optical features of the investigated samples which could not be probed unambiguously with current state-of-the-art time-resolved techniques and data evaluation models. These claims are further validated and quantified by directly comparing experimental data with Monte Carlo simulations. The main advantages offered by our experimental technique, as well as other possible applications, are discussed in the last paragraph.

Limited thickness artifacts We firstly test our setup with the simplest possible disordered slab, a homogeneous isotropic sample made of TiO_2 nanoparticles embedded in a polymer matrix (see SI). Both the nanoparticles and polymer employed are known to have vanishing absorption at the probe wavelength (810 nm). Sample thickness is 203 μm with an average refractive index at 810 nm of 1.52.

Figure 2a shows a typical time-resolved transmission profile along with a fit with the diffusive approximation relation, showing excellent agreement with the experimental data. The fit is performed upon data normalization with the diffusion coefficient D and absorption coefficient $\mu_a = l_a^{-1}$ as the only free parameters, assuming $D = l_t v/3$ and $v = c/n$. The fit returns $l_t = 24.1 \mu\text{m}$ and $l_a = 12.0 \text{ mm}$ (albedo 0.998). The ratio between the thickness of the slab and its transport mean free path (referred to as the optical thickness (OT)) is commonly used as a figure of merit to express the amount of multiple scattering in the sample. According to the fit we obtained an optical thickness of roughly 8.4, with 8 being usually considered as a rule-of-thumb lower limit above which the diffusive transport is regarded as an acceptable approximation⁴⁵. Nonetheless, the retrieved coefficients surprisingly predict a total absorption of $A \sim 8 \%$, which is incompatible with the vanishing absorption expected for both the host polymer and the TiO_2 nanoparticles. Notably, the experimental asymptotic lifetime ($\tau = (6.01 \pm 0.08) \text{ ps}$) is lower than the lowest possible lifetime predicted by diffusion theory for a non-absorbing sample with this refractive index and thickness ($\tau_{\min}^{\text{DA}} = 6.23 \text{ ps}$, cfr. Fig. 2a, inset). The diffusive approximation accommodates for such discrepancy by introducing an absorption artifact: this can be intuitively seen from its relation for the asymptotic decay lifetime $\tau^{-1} = \pi^2 D/L_{\text{eff}}^2 + \mu_a v$ (where L_{eff} is the effective thickness depending on the refractive index boundary conditions), whose value can indeed be made arbitrarily shorter by assuming the presence of absorption.

In this circumstance the analysis of the mean square width evolution is particularly interesting, in that it is inherently free from this absorption-to-scattering crosstalk effect^{13,46,47}. We therefore further investigated the sample switching to our imaging configuration (which, as it is worth noting, could in principle also substitute the photon counter upon frame integration, cfr. Fig. 2b). The mean square width as extracted by the obtained frames clearly shows a linear increase (Figs. 2c-d) that can be easily interpreted within the diffusive approximation, which predicts $w^2(t) = 4Dt$. The experimental slope returns $D_{\text{exp}}^{\text{fit}} = 1746 \mu\text{m}^2 \text{ ps}^{-1} \rightarrow l_t = 26.6 \mu\text{m}$, which is appreciably larger than the value retrieved from the time-resolved curve. We therefore resort to Monte Carlo simulations trying to resolve such discrepancy, eventually succeeding in reproducing simultaneously with a *single* transport parameter l_t both the time-resolved and mean square width evolution data sets as extracted from the ultrafast frames (Figs. 2b and d). A

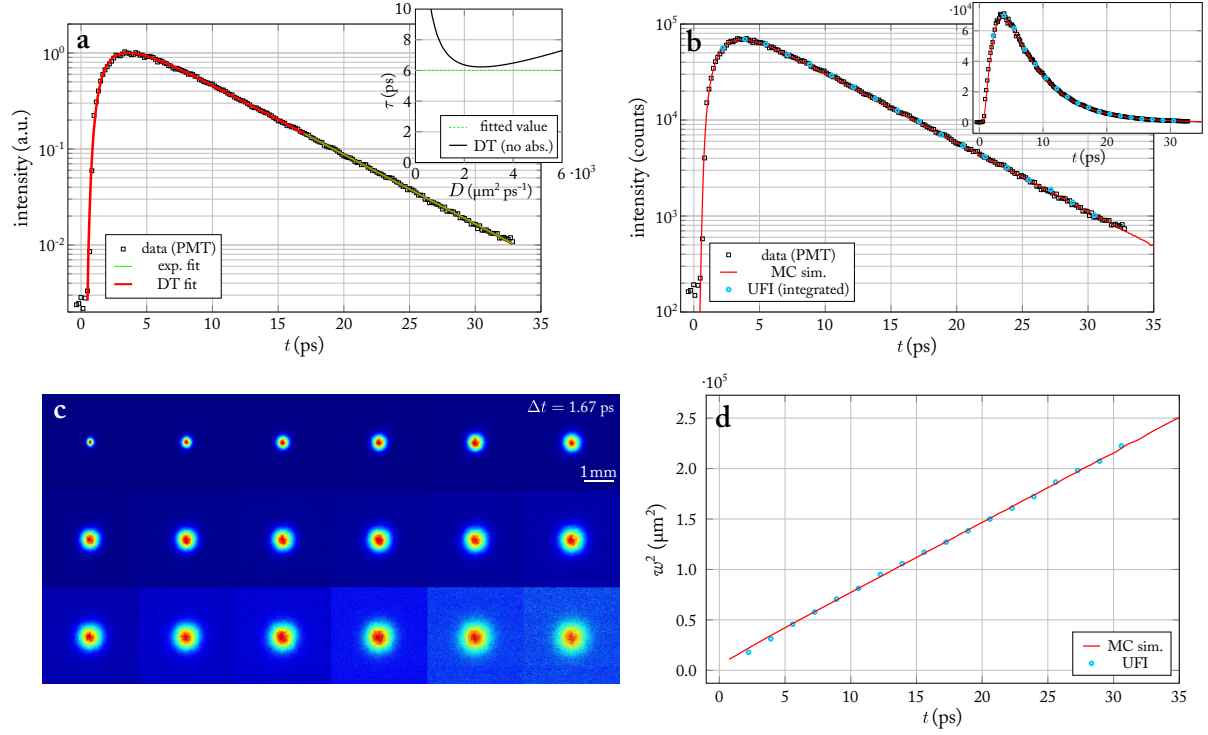


Figure 2: Homogeneous sample data analysis. **a** Experimental data (black squares) acquired with the PMT compared to an exponential fit (green, solid) and a diffusion theory fit with D and μ_a as free parameters (red, solid). Inset shows the asymptotic lifetime expected according to the DA for a sample with $L = 203 \mu\text{m}$, $n = 1.52$ and $\mu_a = 0 \mu\text{m}^{-1}$ (black, solid). The experimentally retrieved value (green, dashed) is incompatible with the DA unless some absorption is introduced. **b** A MC solution (red, solid) of the RTE showing perfect agreement with experimental data for a non-absorbing sample. Integrated intensity from UFI frames is shown along with PMT data as cyan circles. **c** Set of frames acquired at different delays with our UFI setup. Each frame is displayed normalized to its own maximum intensity and results from averaging over different realizations of disorder. **d** Comparison between the experimental and simulated MSW.

Monte Carlo inversion procedure succeeds returning a value of $l_t = 25.5 \mu\text{m}$ (corresponding to a OT ~ 8) perfectly compatible with both datasets without the need to introduce any absorption.

It is worth noting that the transport parameter as retrieved from the mean square width slope in the diffusive framework results in just a 4 % overestimation of the actual MC best value. Such a level of accuracy is acceptable in a wide number of applications, where a UFI technique could be exploited to profitably extend the applicability of the diffusive approximation in this intermediate thickness range without the need to run any simulation. Moreover, as widely suggested in the literature^{46,47}, estimating transport properties from the mean square width rather than from time-resolved data is way more accurate and straightforward, since in the former case prior knowledge of the exact time origin, absorption coefficient, refractive index contrast and sample thickness is not required. Notably, for the same reason that makes the MSW independent of absorption, it is effectively also independent of the integration time as well as of any laser power fluctuation. Interestingly, we unveiled how deceptively the time-resolved diffusive approximation can compensate for its limited accuracy by introducing an absorption artifact, while lacking any real solution when the correct value of absorption is considered. This is a crucial aspect for the optical investigation of optically thin specimens, such as biological tissues⁴⁸.

As already mentioned, our UFI technique is capable of replacing completely integrated measurements with comparable sensitivity (cfr. Fig. 2b). The resulting set of frames can be conveniently decomposed into a MSW and a time-resolved curve, thus providing in a single measurement session two almost independent data sets. Indeed, the former does not depend on the integrated intensity of single frames, while the latter is mainly linked to the transport along the z axis. In this respect our perfectly matching Monte Carlo validation, which is carried independently on two experimental data sets which depend differently on different sets of parameters, is a clear indication of the quantitative accuracy and reliability of our setup over many orders of magnitude both in the temporal and spatial domain.

Large scale heterogeneity artifacts We took advantage of our UFI technique to investigate diverse and more complex media. A new polymer slab ($L = 190 \mu\text{m}$) with a roughly doubled scatterer density was made in order to obtain an optically thicker sample. Again, a perfect fit could be obtained in the diffusive framework (Fig. 3a) only if accounting for the presence of absorption up to an unlikely integrated value of $A \sim 7\%$ ($l_t = 12 \mu\text{m}$, $l_a = 13.2 \text{ mm}$). In sharp contrast with the previous experiment, this time a non-absorbing Monte Carlo fit was also unable to reproduce the time-resolved data even when perfectly matching the observed experimental lifetime (Fig. 3b, black dotted line). Regarding the mean square width, on the other hand, it exhibited a steeper than expected slope ($D_{\text{exp}}^{\text{fit}} = 1050 \mu\text{m}^2 \text{ ps}^{-1} \rightarrow l_t = 16 \mu\text{m}$) as if the diffusion process was enhanced along in-plane directions, as shown in Figure 3c.

In order to resolve this discrepancy we further investigated the sample with a Scanning Electron Microscope (SEM), revealing a heavily layered modulation of the scatterer density, as compared to the more homogeneously dispersed one of our first sample (Figs. 4a and b). Taking advantage of the versatility of Monte Carlo simulations we modeled our sample after our SEM images as being composed by 5 layers of 3 different thicknesses and densities, arranged symmetrically with respect to the central layer. A new MC brute force fit with fixed

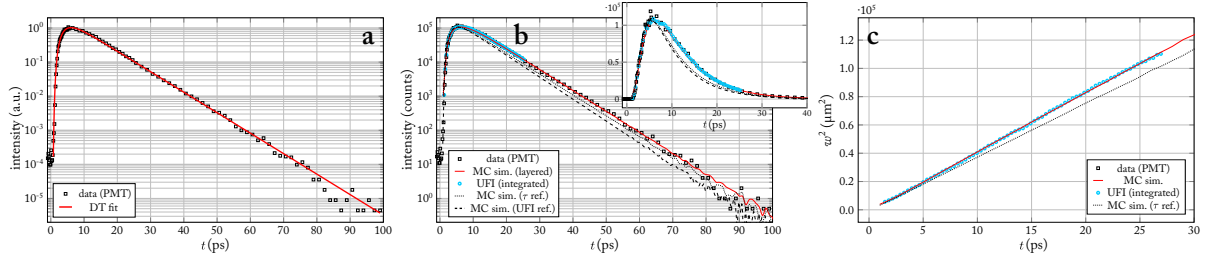


Figure 3: Heterogeneous sample data analysis. **a** PMT data (black squares) and best DA fit (red, solid), returning $l_t = 12 \mu\text{m}$ and $l_a = 13.2 \text{ mm}$. **b, c** Comparison between the PMT and UFI data with a multi-layered simulation (solid, red) and two *homogeneous* simulations. The black dotted line refers to the simulation that was able to reproduce the experimental lifetime ($l_t = 14.2 \mu\text{m}$), while the black dashed line shows the simulation that was able to reproduce the MSW slope ($l_t = 15.7 \mu\text{m}$). The lifetime-reproducing simulation fails to reproduce the MSW slope, while the simulation that shows perfect agreement with the MSW slope poorly matches the time-resolved decay, thus revealing the inconsistency of the homogeneity hypothesis. MC decays have been rescaled to match the experimental peak counts value.

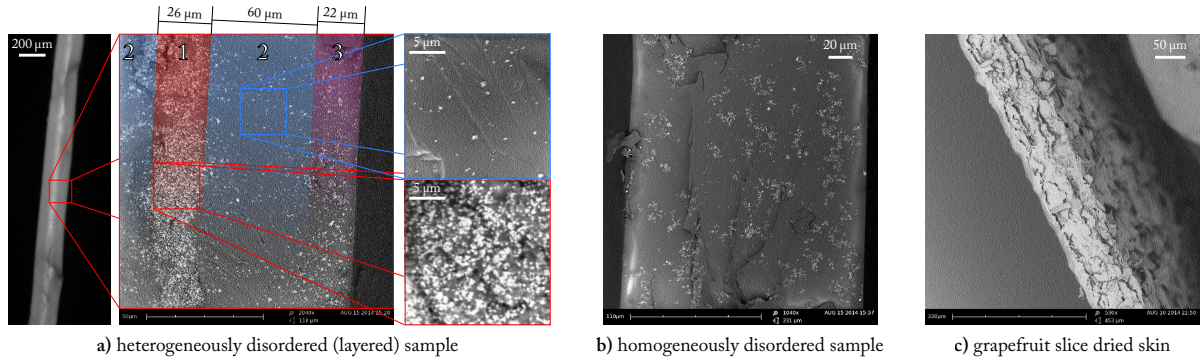


Figure 4: SEM side-view images of analyzed samples. **a** The central inset shows the section of our heterogeneous sample, which exhibits a layered symmetric structure that we modeled with a high density central layer ($L_1 = 26 \mu\text{m}$), a low density interstitial layer ($L_2 = 60 \mu\text{m}$) and an intermediate density outer layer ($L_3 = 22 \mu\text{m}$). The heterogeneity represented by the core layer is appreciable also at the optical microscope (left inset). Right insets qualitatively highlight the density difference between regions 1 and 2. **b** Transverse section of the reference sample: although showing signatures of scatterer clustering, small scale clusters/heterogeneities are homogeneously dispersed across the sample thickness, and does not exhibit any layered arrangement. As confirmed by the excellent agreement obtained with a single parameter MC simulation, light sees an effective, homogeneous scatterer density in contrast to the tightly layered one of the previous sample, as also confirmed by other works on similar samples⁴⁹. **c** Lateral section of the grapefruit slice dried skin.

geometry and three free parameters l_{t1} , l_{t2} , l_{t3} was eventually able to perfectly reproduce both time-resolved and MSW data simultaneously, as shown in Figures 3b-c. We retrieved transport mean free paths of $l_{t1} = 3.5 \mu\text{m}$, $l_{t2} = 21.5 \mu\text{m}$ and $l_{t3} = 11 \mu\text{m}$ respectively for the high, low and intermediate density layers. Absorption coefficients were all set to $\mu_a = 0 \mu\text{m}^{-1}$. In this case, the MSW/time-resolved decomposition clearly allowed to reveal and characterize an unexpected degree of complexity thanks to the rigid constraints cast by the double boundary datasets. Notably, resolving this composite structure showed that a layered heterogeneity can in principle mimic the effects of anisotropic transport, thus revealing a yet unaddressed physical effect (and engineering degree of freedom) to be aware of. This is especially relevant given the pervasiveness of layered media (coatings, atmospheric physics, biological tissues, etc.), which often exhibit counter-intuitive features that standard time-resolved techniques are still unable to elucidate, as in the case of light transport across the human forehead⁵⁰.

Ultrathin samples Despite the advantages offered by the MSW/time-resolved decomposition, it is clear that actually the raw, non-integrated data provide an irreducible set of information. A dramatic illustration of this point is obtained by studying a thin biological sample such as a small strip cut from the dried skin of a grapefruit slice. As the SEM image revealed (Figure 4c), its structure is made of a conglomerate of small flakes forming a corrugated slab approximately $85 \mu\text{m}$ thick. The dried sample appears as a brittle, almost transparent membrane (Figure 5a, inset).

In this range of optical (and absolute) thicknesses, standard experimental techniques come short because of the extreme time scales involved, causing the common diffusive modeling to fail drastically. Moreover, most of the signal will be ballistically transmitted bringing almost no information about the optical properties of the sample. As Figure 5a shows, the light that is scattered inside the grapefruit membrane is less than 1/50th of the original intensity. Our ultrafast imaging technique allows us to selectively address the light that was held for longer inside the sample, while at the same time spatially inspecting it as it propagates along the main (transverse) slab extension. Figure 5b shows a collection of frames acquired over a time window of roughly 5 ps after pulse injection, corresponding to a total pathlength $\gtrsim 13$ times the sample thickness. We see that light spreads through the membrane with a well defined wavefront traveling inside its main plane, resulting in a dramatic departure from any prediction compatible with the diffusive framework. Yet, it should be noted that standard time-resolved or steady-state investigations would still just measure a decaying lifetime and a bell-shaped profile respectively, which could deceptively support an inappropriate interpretation in terms of the diffusive approximation.

As we will show, our ultrafast time- and space-resolved experiment provides also in this case a deep insight in the light transport properties of complex systems which requires the development of a novel analysis methodology. We demonstrate a proof-of-concept procedure to assess in-plane transport properties in this extremely optically thin regime. For the sake of simplicity we will illustrate our investigation on a cross-cut of the profile assuming isotropic transport. The general treatment is analogue and will be object of future works. Figure 5c shows a comparison between experimental cross-cuts at different instants and the corresponding time evolution of an isotropic Monte Carlo simulation which succeeds in reproducing the wavefront

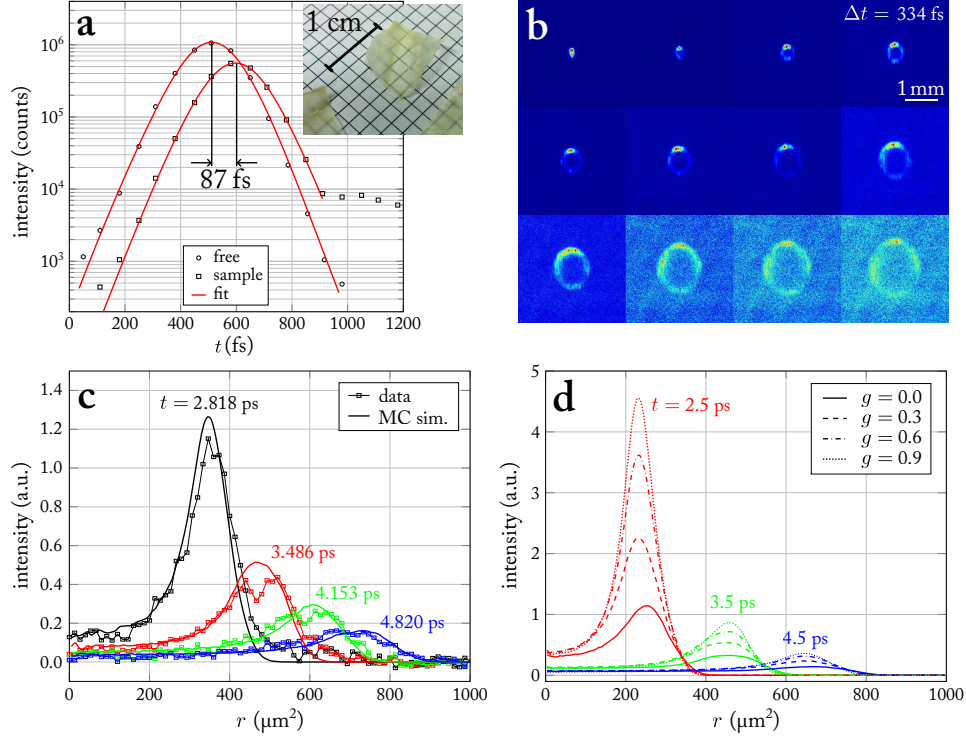


Figure 5: Grapefruit skin data analysis. **a** Time shift induced by the sample in the probe path (black circles vs. black squares). Knowing its thickness by previous SEM measurements, an effective refractive index can be retrieved as $n = 1 + c\Delta t/L \sim 1.31$. Inset shows actual appearance of investigated specimens. **b** Frames set, each of which is integrated over a small portion of the sample. The transmitted intensity distribution shows a quasi ballistic elliptic wavefront traveling at slightly different speeds (see SI). **c** Horizontal cross-cuts of the wavefront and MC fit with g and l_s as free parameters. The fit returns values of $g = 0.7$ and $l_s = 150 \mu\text{m}$. **d** Simulated radial intensity profiles in this extremely optically thin regime shows a heavy breakdown of the similarity relation.

speed, intensity decay and overall shape at all given times. To achieve this collective agreement it is required to consider also the anisotropic scattering coefficient g as an additional parameter, expressing the degree of directional correlation between consecutive scattering events. As already mentioned, diffusion theory is degenerate on g as long as the transport mean free path l_t is kept constant, which is expressed by the similarity relation $l_t = l_s/(1 - g)$. This is why retrieving any information on the angular scattering function is particularly challenging, and one must necessarily resort to some angular, spatial or temporal regime where the diffusive approximation ceases to hold⁴⁴. Indeed, as shown by Figure 5d, the observed transverse intensity patterns exhibit a large breakdown of this degeneracy condition in such thin slabs, with g playing a substantial role in determining the shape and evolution of the traveling wavefront even when keeping l_t constant. In particular, while the outer wavefront propagates almost ballistically (see SI), its instantaneous position and peak intensity vary sensibly with different combinations of g and l_s , thus allowing a retrieval of both with an estimated precision of roughly 10 %. The set of simulated curves shown in Figure 5c is obtained for $g = 0.7$ and $l_s = 150 \mu\text{m}$ (corresponding to an in-plane $l_t = 500 \mu\text{m}$), although we must keep in mind that quantitatively accurate figures for this particular specimen would require an analysis involving fully anisotropic simulations.

The main purpose of this experiment aims at showcasing the vast possibilities opened by such a rich time- and space-resolved output. In this respect it is worth noting that our g estimation results from a collective fitting routine involving multiple spatio-temporal data sets, which stands in contrast with common and less robust g determination techniques involving a single scalar, such as for example the attenuation coefficient of a collimated beam^{51,52}. Accurate determination of single scattering anisotropy is crucial to directly probe the shape, orientation and optical properties of single microscopic scatterers, and might therefore prove of significant interest in a broad range of fields, from photo-therapeutic diagnostics⁵³ to realistic computer rendering of participating media^{54,55}. Moreover, as opposed to other available techniques, determination of g and l_s is achieved from a single measurement session, which also simplifies the retrieval procedure. The peculiar doughnut-shaped intensity pattern that enables such a rich characterization of scattering properties is of course not unique to this particular sample, as we were able to observe it in a variety of different biological samples — both of plant and animal origin — usually differing just by the actual contour shape of the propagating wavefront. This brings supporting evidence that our proof-of-concept evaluation technique has general validity and will prove useful in studying extremely complex media, included biological tissues.

Discussion As illustrated in the previous paragraphs, our optically-gated imaging technique offer several advantages. From a technical viewpoint, one main strength of our setup is its simplicity and lack of complex electronics. The inherently synchronous nature of the pulses makes the whole setup insensitive to timing jitter. Power fluctuation/drifts do not pose a problem as well when measuring the mean square width evolution, which also allows to adjust dynamically the integration time to enhance the signal-to-noise ratio. This flexibility should make possible to replicate the setup with cheaper and more easily usable hands-off fiber lasers, thus widening the effective applicability of the technique.

Accessing both transverse and axial transport simultaneously allows to correctly evaluate

the applicability of the common diffusion framework, which can be subject to appreciable absorption overestimation in samples presenting a limited optical thickness or large scale heterogeneities. An accurate retrieval of the absorption coefficient is particularly relevant in many biomedical applications where its value is directly linked to e.g. chromophores concentration or blood oxygenation levels. The observed discrepancy, which would be not apparent with state-of-the-art spatial or temporal measurements, is revealed by comparing a standard time-resolved transmitted intensity decay with the evolution of the mean square width, both of which can be acquired simultaneously. Nevertheless, the most relevant advantage offered by a direct access to the transient mean square width expansion is that it enables a robust and simple interpretation. In sharp contrast with other common observables such as the total transmittance and its decaying lifetime, the mean square width is in fact exactly independent from absorption and also largely unaffected by different refractive index contrasts and sample thicknesses, thus overcoming the longstanding problem posed by their precise assessment. One prominent case where this feature could be decisive is that of the experimentally observed decrease in the diffusive coefficient of a turbid slab with decreasing thickness⁵⁶, which was determined indirectly through the transmittance decay lifetime. A spatio-temporal measurement would allow to directly probe the diffusion coefficient irrespective of the exact boundary conditions, whose incorrect assessment has been adduced as a possible cause for this apparently anomalous behavior³³.

A different scenario emerges when studying samples with extremely low optical thickness, which revealed a peculiar transport regime where l_s and g , rather than l_t , are the only meaningful parameters to determine how radiative energy spreads through the sample. This further illustrates how there exist practical situations where light transport must necessarily be studied as a spatio-temporal phenomenon in its entirety, a point that to our knowledge has not been properly considered so far when studying transport in thin samples. Moreover, we demonstrated how this transport regime enables accurate retrieval of otherwise hardly accessible transport parameters, especially for this class of samples where well-established experimental techniques are still missing.

More in general, several applications are enabled by the three-dimensional characterization capabilities of the setup (see also SI), opening new possibilities to investigate anisotropic media whose correct modeling is currently object of a lively debate in the literature^{16,57,58}. Other relevant open questions that might be tackled directly with a spatio-temporal investigation might include an experimental verification of the polarization dependence predicted for the diffusion coefficient⁵⁹ as well as of the occurrence of a non-monotonic mean square width evolution in samples exhibiting Anderson localization⁴⁶ or the lateral expansion of Lévy type transport, where the inherent truncation length given by the slab thickness might be eluded⁶⁰. Similarly, a reflection UFI measurement on macro-porous bulk materials could access light spreading within the first few hundred femtoseconds, from which the time-dependent diffusion constant could be retrieved¹⁶ bringing information on the structure factor of the material which would be hardly obtainable at long times.

Conclusions

The field of light transport in complex or structured media still presents a multitude of experimental challenges that could largely benefit from the advent of novel multi-domain investigation techniques. In this work, we have demonstrated an experimental technique to go beyond the ps-resolution barrier for spatial investigation of transient intensity profiles emerging from arbitrary samples. Gaining access to this time scale with a broad field of view is key to the study of a broad class of samples, ranging from thin biological membranes to complex optical microdevices. As we demonstrated, spatio-temporal investigations play an enabling role in the study of broad classes of samples such as heterogeneous or semitransparent media which we could hardly characterize with present state-of-the-art techniques. Also when dealing with more standard samples, combined access to both transverse and axial transport helps revealing the presence of flaws or artifacts in the common diffusion-based data evaluation framework. Remarkably, in many practical situations we found that low optical thickness can be exploited as an advantage rather than a drawback, therefore offering a complementary framework to study also that broad class of samples that do not meet the validity conditions required by the diffusion approximation. Nonetheless, the setup that we propose is clearly one of extremely general purpose being non-invasive, usable at different wavelengths, with a broad field of view and high time-resolution. We therefore envision that it could be profitably applied in a wide range of photonic applications both for the sub-ps physics that it allows to investigate and for the convenient wide field acquisition which does not require scanning over the region of interest.

Acknowledgements We wish to thank G. Mazzamuto, F. Utel and J. Bertolotti for technical assistance and T. Svensson, E. Alerstam, S. Gigan and P. Wasylczyk for fruitful discussions. This work is financially supported by the European Network of Excellence Nanophotonics for Energy Efficiency and the ERC through the Advanced Grant PhotBots (proj. ref. 291349).

Author Contributions M.B., L.P. and R.S. conceived and carried out the time-resolved experiments. L.P. and R.S. realized the samples, L.P. ran the simulations. All authors discussed the results and contributed to the writing of the paper.

Competing Interests The authors declare that they have no competing financial interests.

Correspondence Correspondence and requests for materials should be addressed to L.P. (pattelli@lens.unifi.it).

References

1. Drexler, W. *et al.* Ultrahigh-resolution ophthalmic optical coherence tomography. *Nature medicine* **7**, 502–507 (2001).
2. Obrig, H. & Villringer, A. Beyond the visible—imaging the human brain with light. *Journal of Cerebral Blood Flow & Metabolism* **23**, 1–18 (2003).
3. Dunsby, C & French, P. Techniques for depth-resolved imaging through turbid media including coherence-gated imaging. *Journal of Physics D: Applied Physics* **36**, R207 (2003).

4. Engelen, R. J. *et al.* Ultrafast evolution of photonic eigenstates in k-space. *Nature Physics* **3**, 401–405 (2007).
5. Minardi, S *et al.* Three-dimensional light bullets in arrays of waveguides. *Physical review letters* **105**, 263901 (2010).
6. Bassi, A. *et al.* Time-gated optical projection tomography. *Optics letters* **35**, 2732–2734 (2010).
7. Velten, A. *et al.* Recovering three-dimensional shape around a corner using ultrafast time-of-flight imaging. *Nature Communications* **3**, 745 (2012).
8. Eggebrecht, A. T. *et al.* Mapping distributed brain function and networks with diffuse optical tomography. *Nature Photonics* (2014).
9. Gao, L., Liang, J., Li, C. & Wang, L. V. Single-shot compressed ultrafast photography at one hundred billion frames per second. *Nature* **516**, 74–77 (2014).
10. Nakagawa, K *et al.* Sequentially timed all-optical mapping photography (STAMP). *Nature Photon.* **8**, 695–700 (2014).
11. Li, Z., Zgadzaj, R., Wang, X., Chang, Y.-Y. & Downer, M. C. Single-shot tomographic movies of evolving light-velocity objects. *Nature communications* **5** (2014).
12. Gundlach, L. & Piotrowiak, P. Femtosecond Kerr-gated wide-field fluorescence microscopy. *Optics letters* **33**, 992–994 (2008).
13. Sperling, T., Buehrer, W., Aegerter, C. M. & Maret, G. Direct determination of the transition to localization of light in three dimensions. *Nature Photon.* **7**, 48–52 (2012).
14. Farid, N, Harilal, S., Ding, H & Hassanein, A. Dynamics of ultrafast laser plasma expansion in the presence of an ambient. *Applied Physics Letters* **103**, 191112 (2013).
15. Grumstrup, E. M., Gabriel, M. M., Cating, E. E., Van Goethem, E. M. & Papanikolas, J. M. Pump–probe microscopy: Visualization and spectroscopy of ultrafast dynamics at the nanoscale. *Chemical Physics* **458**, 30–40 (2015).
16. Svensson, T. *et al.* Light diffusion in quenched disorder: Role of step correlations. *Physical Review E* **89**, 022141 (2014).
17. Shah, J. Ultrafast luminescence spectroscopy using sum frequency generation. *Quantum Electronics, IEEE Journal of* **24**, 276–288 (1988).
18. Yodh, A., Kaplan, P. & Pine, D. Pulsed diffusing-wave spectroscopy: High resolution through nonlinear optical gating. *Physical Review B* **42**, 4744 (1990).
19. Trebino, R. *Frequency-Resolved Optical Gating: The Measurement of Ultrashort Laser Pulses* (Springer, 2000).
20. Savo, R., Burresi, M., Svensson, T., Vynck, K. & Wiersma, D. S. Walk dimension for light in complex disordered media. *Physical Review A* **90**, 023839 (2014).
21. Burresi, M. *et al.* Bright-White Beetle Scales Optimise Multiple Scattering of Light. *Scientific reports* **4** (2014).
22. Potenza, M. A. *et al.* Three dimensional imaging of short pulses. *Optics communications* **229**, 381–390 (2004).
23. Firester, A. Image upconversion: part III. *Journal of Applied Physics* **41**, 703–709 (1970).

24. Chiou, W. Geometric optics theory of parametric image upconversion. *Journal of Applied Physics* **42**, 1985–1993 (1971).
25. Faris, G. W. & Banks, M. Upconverting time gate for imaging through highly scattering media. *Optics letters* **19**, 1813–1815 (1994).
26. Devaux, F & Lantz, E. Ultrahigh-speed imaging by parametric image amplification. *Optics communications* **118**, 25–27 (1995).
27. Abraham, E. *et al.* Real-time two-dimensional imaging in scattering media by use of a femtosecond Cr^{4+} :forsterite laser. *Opt. Lett.* **25**, 929–931 (2000).
28. Lantz, E. & Devaux, F. Parametric amplification of images: from time gating to noiseless amplification. *Selected Topics in Quantum Electronics, IEEE Journal of* **14**, 635–647 (2008).
29. Pedersen, C., Karamehmedović, E., Dam, J. S. & Tidemand-Lichtenberg, P. Enhanced 2D-image upconversion using solid-state lasers. *Optics express* **17**, 20885–20890 (2009).
30. Dam, J. S., Pedersen, C. & Tidemand-Lichtenberg, P. High-resolution two-dimensional image upconversion of incoherent light. *Optics letters* **35**, 3796–3798 (2010).
31. Graaff, R., Aarnoudse, J. G., de Mul, F. F. & Jentink, H. W. Similarity relations for anisotropic scattering in absorbing media. *Optical engineering* **32**, 244–252 (1993).
32. Van de Hulst, H. C. *Multiple light scattering: tables, formulas, and applications* (Elsevier, 2012).
33. Elaloufi, R., Carminati, R. & Greffet, J.-J. Time-dependent transport through scattering media: from radiative transfer to diffusion. *Journal of Optics A: Pure and Applied Optics* **4**, S103 (2002).
34. Xu, M, Cai, W, Lax, M & Alfano, R. Photon migration in turbid media using a cumulant approximation to radiative transfer. *Physical Review E* **65**, 066609 (2002).
35. Garofalakis, A. *et al.* Characterization of the reduced scattering coefficient for optically thin samples: theory and experiments. *Journal of Optics A: Pure and Applied Optics* **6**, 725 (2004).
36. Hammer, M, Roggan, A, Schweitzer, D & Muller, G. Optical properties of ocular fundus tissues-an in vitro study using the double-integrating-sphere technique and inverse Monte Carlo simulation. *Physics in medicine and biology* **40**, 963 (1995).
37. Kienle, A. & Patterson, M. S. Determination of the optical properties of turbid media from a single Monte Carlo simulation. *Physics in medicine and biology* **41**, 2221 (1996).
38. Pifferi, A., Taroni, P., Valentini, G. & Andersson-Engels, S. Real-time method for fitting time-resolved reflectance and transmittance measurements with a Monte Carlo model. *Applied optics* **37**, 2774–2780 (1998).
39. Alerstam, E., Andersson-Engels, S. & Svensson, T. White Monte Carlo for time-resolved photon migration. *Journal of biomedical optics* **13**, 041304–041304 (2008).
40. Leonetti, M. & López, C. Measurement of transport mean-free path of light in thin systems. *Optics letters* **36**, 2824–2826 (2011).
41. Nilsson, A. M., Berg, R. & Andersson-Engels, S. Measurements of the optical properties of tissue in conjunction with photodynamic therapy. *Applied optics* **34**, 4609–4619 (1995).
42. Dam, J. S., Yavari, N., Sørensen, S. & Andersson-Engels, S. Real-time absorption and scattering characterization of slab-shaped turbid samples obtained by a combination of angular and spatially resolved measurements. *Applied optics* **44**, 4281–4290 (2005).

43. Karlsson, H., Fredriksson, I., Larsson, M. & Strömberg, T. Inverse Monte Carlo for estimation of scattering and absorption in liquid optical phantoms. *Optics express* **20**, 12233–12246 (2012).
44. Svensson, T. *et al.* Exploiting breakdown of the similarity relation for diffuse light transport: simultaneous retrieval of scattering anisotropy and diffusion constant. *Optics letters* **38**, 437–439 (2013).
45. Elaloufi, R., Carminati, R. & Greffet, J.-J. Diffusive-to-ballistic transition in dynamic light transmission through thin scattering slabs: a radiative transfer approach. *JOSA A* **21**, 1430–1437 (2004).
46. Cherroret, N, Skipetrov, S. & Van Tiggelen, B. Transverse confinement of waves in three-dimensional random media. *Physical Review E* **82**, 056603 (2010).
47. Hu, H., Strybulevych, A., Page, J. H., Skipetrov, S. E & van Tiggelen, B. A. Localization of ultrasound in a three-dimensional elastic network. *Nature Physics* **4**, 945–948 (2008).
48. Tuchin, V. V. & Tuchin, V. *Tissue optics: light scattering methods and instruments for medical diagnosis* (SPIE press Bellingham, 2007).
49. Vos, W. L., Tukker, T. W., Mosk, A. P., Lagendijk, A. & IJzerman, W. L. Broadband mean free path of diffuse light in polydisperse ensembles of scatterers for white light-emitting diode lighting. *Applied optics* **52**, 2602–2609 (2013).
50. Comelli, D. *et al.* In vivo time-resolved reflectance spectroscopy of the human forehead. *Applied optics* **46**, 1717–1725 (2007).
51. Marchesini, R., Bertoni, A, Andreola, S, Melloni, E & Sichirollo, A. Extinction and absorption coefficients and scattering phase functions of human tissues in vitro. *Applied Optics* **28**, 2318–2324 (1989).
52. Pickering, J. W. *et al.* Double-integrating-sphere system for measuring the optical properties of tissue. *Applied optics* **32**, 399–410 (1993).
53. Nilsson, A. M., Stureson, C., Liu, D. L. & Andersson-Engels, S. Changes in spectral shape of tissue optical properties in conjunction with laser-induced thermotherapy. *Applied optics* **37**, 1256–1267 (1998).
54. Pauly, M., Kollig, T. & Keller, A. *Metropolis light transport for participating media* (Springer, 2000).
55. Premože, S., Ashikhmin, M., Tessendorf, J., Ramamoorthi, R. & Nayar, S. in *Proceedings of the Fifteenth Eurographics conference on Rendering Techniques* (2004), 363–374.
56. Kop, R. H., de Vries, P., Sprik, R. & Lagendijk, A. Observation of anomalous transport of strongly multiple scattered light in thin disordered slabs. *Physical review letters* **79**, 4369 (1997).
57. Kienle, A. Anisotropic Light Diffusion: An Oxymoron? *Phys. Rev. Lett.* **98**, 218104 (21 2007).
58. Alerstam, E. Anisotropic diffusive transport: Connecting microscopic scattering and macroscopic transport properties. *Phys. Rev. E* **89**, 063202 (6 2014).
59. Vynck, K., Pierrat, R. & Carminati, R. Polarization and spatial coherence of electromagnetic waves in uncorrelated disordered media. *Physical Review A* **89**, 013842 (2014).
60. Bertolotti, J. *et al.* Engineering disorder in superdiffusive Levy glasses. *Advanced Functional Materials* **20**, 965–968 (2010).

Supplementary Information to: Spatio-temporal visualization of light transport in complex photonic structures

Experimental setup details

The non-linear crystal used is a square $5\text{ mm} \times 5\text{ mm} \times 2\text{ mm}$ BBO crystal. Focal lengths are respectively 100 mm for L2 and L3, and 125 mm for the lens collecting the up-converted signal after the BBO. The final magnification obtained through the double imaging stages was roughly $1\times$. The focusing lens L1 is chosen so to provide a point-like excitation spot with respect to the typical length scales of the sample, which in our case was set to $\sim 10\text{ }\mu\text{m}$. As far as the mentioned constraints on the wavevector distribution manipulation are satisfied, a different set of optics can be employed to obtain a different magnification. The CCD camera is a back-illuminated Andor iKon M912, with a 512×512 pixel sensor.

Polymer samples fabrication

Investigated polymer samples are made of a commercial UV-curing acrylate optical adhesive (Norland 65) with a dispersion of rutile nanoparticles with a diameter of 280 nm (Huntsman's Tiioxide R-XL). The mixture of polymer and nanoparticles is rendered homogeneous through magnetic stirring and an ultrasonic bath ($\sim 1\text{ h}$). We then let the resulting opaque paste be sucked by capillary forces inside an air gap of controlled thickness formed between two microscope glasses. The two glasses are firmly held apart by micro-spherical spacers of calibrated size. By spin coating in advance the microscope glasses with water-soluble polyvinyl alcohol we are able at a later stage to remove the glasses obtaining a flexible, free standing polymer slab. This notably allows to avoid multiple reflection of both pump and scattered light coming from the enclosing glasses.

Monte Carlo software

All simulations shown have been performed with a C++ software called MCPlusPlus¹ based on the standard MCML Monte Carlo code for multi-layered slab samples². Its source code is currently under development and is freely available at <http://www.lens.unifi.it/quantum-nanophotonics/mcplusplus/>. Benefiting from the object-oriented paradigm of C++, the software offers a high level of abstraction, scalability, modularity and ease of maintenance. Being completely written in C++, it can be executed on any hardware and can take extensive advantage of the multi-thread capabilities of most modern CPUs for increased performance. Other features worth mentioning include python scriptability and both raw and histogrammed output in the convenient H5 binary format.

Probe and gate pulses characterization

A Spectra Physics TSUNAMI Ti:Sa laser is used to pump a OPAL optical parametric oscillator, which provides a signal at $(1510 \pm 11)\text{ nm}$, an idler (not used in the experiment) and an

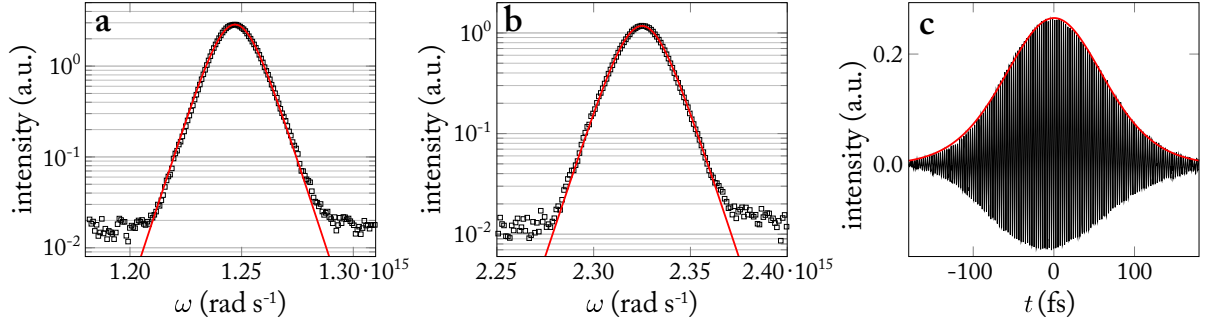


Figure S1: Pulses characterization. **a** Spectrum of the unconverted residual (probe pulse) from the OPO, with a $\text{sech}^2(\omega)$ fit. **b** Spectrum of the OPO signal (gate pulse) with a $\text{sech}^2(\omega)$ fit. **c** Autocorrelation measurement of the residual pulse. The envelope profile fringes has been fitted with the autoconvolution of two $\text{sech}^2(t)$ pulses.

unconverted residual at the same wavelength of the pump (i.e. (810 ± 5) nm). The average power of the signal and the residual beam is respectively 190 mW and 280 mW. Both pulses are characterized at the beginning of each measurement session spectrally and temporally. Figures S1a and b show typical spectra recorded for the TSUNAMI and the OPAL, fitted with a $I(\omega) \propto \text{sech}^2(\frac{\pi}{2}(\omega - \omega_c)\tau_p)$ function, as expected for an actively mode-locked Ti:Sa laser in a sub-ps configuration (i.e. featuring GDD compensation). Figure S1c shows an autocorrelation measurement of the residual pulse, fitted with the autoconvolution of two sech^2 pulses, which can be expressed as $I_{ac}(t) = \gamma \text{cosech}^2(\gamma t) [\gamma \coth(\gamma t) - 1]$ with $\gamma = (2 \log(1 + \sqrt{2})) / (\tau_{fwhm})$. The full width half maximum duration of the original pulse is obtained by multiplication for the appropriate deconvolution factor, giving $\tau_{fwhm} = 0.6482 \times 144.6 \text{ fs} = 93.7 \text{ fs}$. To estimate the duration of the gate pulse we can rely on the cross-correlation measurement. Due to the lack of any analytical expression for the cross-convolution of two different sech^2 pulses, we performed a fit plugging at each iteration the numerical convolution of the known pump pulse with an unknown sech^2 pulse (Fig. 1b). The routine eventually returned a full width duration of 134 fs for the gate pulse. The cross-correlation was measured with and without the lenses, to make sure that the optics used for the experiment were introducing negligible dispersion. The final full width half maximum, representing the instrument response function is of approximately 170 fs. The source term in all Monte Carlo simulation showed in this paper has been modeled as a sech^2 pulse of this duration, while its spatial distribution was set to a Gaussian beam with a waist of $10 \mu\text{m}$, as given by our focusing lens.

Full 3D retrieval of ballistic speed of light

Spatio-temporal measurements of light traveling inside the grapefruit membrane and other analogue samples exhibit a transmitted intensity pattern which is determined by both ballistic and scattered light — where by “ballistic” we refer to light that undergoes roughly just two main scattering events: one to get inside the membrane and one to be scattered out. In particular, such ballistic component appears to persist for the whole time scale observed in our experiment and can be easily addressed by measuring the instantaneous position of the outer wavefront of

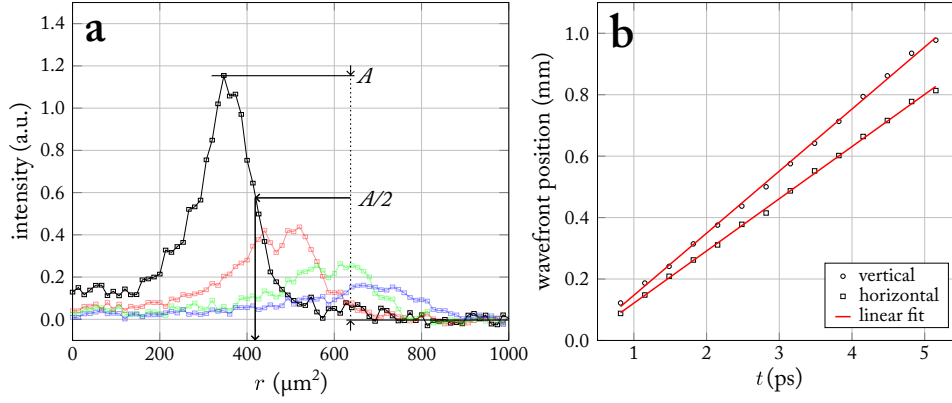


Figure S2: Grapefruit in-plane light speed retrieval. **a** For each measured profile, the instantaneous position of its outer wavefront is calculated at half its maximum amplitude A for both horizontal (shown) and vertical cross-cuts. **b** For the whole time window taken into account by our measurements the outer wavefront appears to travel ballistically with a well-defined speed. Linear fits return speeds of $170 \mu\text{m ps}^{-1}$ ($0.57c$) and $200 \mu\text{m ps}^{-1}$ ($0.67c$) for the horizontal and vertical axis respectively.

the traveling pulse where, by definition, it is accumulated. This is confirmed by the steadily linear increase of the wavefront position. The retrieved slopes directly give the light speed along a certain direction inside the slab specimen, which notably appears to be different along the x and y direction for the investigated sample. Combining these results with the perpendicular delay introduced by the intervening sample whose thickness is known (cfr. Figure 5a) we are able to retrieve the speed of light inside the membrane along each spatial dimension.

References

1. Mazzamuto, G. & Pattelli, L. *MCPlusPlus Documentation* <<http://www.lens.unifi.it/quantum-nanophotonics/mcplusplus/>> (2015).
2. Wang, L., Jacques, S. L. & Zheng, L. MCML—Monte Carlo modeling of light transport in multi-layered tissues. *Computer methods and programs in biomedicine* **47**, 131–146 (1995).